J Mater Sci (2006) 41:6760–6767
DOI 10.1007/s10853-006-0215-4

# Micro/macro-mechanical approach of first ply failure in CFRP

**Bodo Fiedler · Claas de Jong · Thomas Hobbiebrunken · Masaki Hojo · Karl Schulte**

Published online: 19 August 2006


**Abstract** A combined experimental and numerical study has been carried out in order to predict initial failure in transversely loaded carbon fibre/epoxy composites. Three-point bending experiments on macroscopic composite specimens with special laminate lay-ups were carried out in a scanning electron microscope (SEM). The in-situ experiments allow observing the onset of microscopic composite failure under transverse loading and measurement of the global applied load at onset of failure. The experimental results show that interfacial failure was the dominating failure mechanism. The interfacial stresses at initiation of failure were determined successfully by a non-linear micro/macro FE-Analysis and compared with experimental results obtained from 3-point bending tests of standard composite specimens. The results show that the interfacial normal strength (INS) governs the failure process.

## Introduction

The study of composite failure initiation is a topic of major interest. Composite failure initiation is a complex topic based on various failure mechanisms and the factors that occur successively and/or at the same time. Composite materials exhibit hierarchical internal structures over a wide range of the length-scales (compare Fig. 1) and a failure analysis must regard the complex internal structure [1]. For example on the micro scale the composite consists of fibres and matrices bonded together to form individual plies. The fibres and matrix are considered as homogenous and continuous materials in a microscopic analysis of composite materials. Those plies are bonded together to form a laminate in which the fibres in each ply are oriented in different directions. On the macro scale a structural component made of a composite laminate also appears homogeneous.

A certain hierarchical level usually controls a property in the higher levels (although a property can be controlled by several levels) and strongly depends on the interactions with the lower levels [2]. The deformation and failure behaviour of such hierarchical materials can be understood using a multi-scale approach that deals with the different size scales, which appear in the composite. The effective elastic deformation properties for linear elastic composites have been addressed extensively in history. Pioneering works were performed by Voigt [3] and Reuss [4]. Where the Voigt approach gives upper bounds and the Reuss approximation gives lower bounds of the elastic moduli. These early works yielded the most famous basic theory, which is today known as the rule of mixtures (ROM). Other works use self consistent methods [5], variational methods [6–9] and exact or unit-cell methods [9, 10].

All these methods provide homogenized properties of the heterogeneous material under consideration. When the failure of composite materials is considered, it is necessary to compute the stresses and strains not only at the macro-scale but also at the characteristic mesoscale or microscale,

B. Fiedler (✉) · C. de Jong · K. Schulte
Institute of Polymer Composites,
Technische Universität Hamburg-Harburg,
Hamburg-Harburg, Germany
e-mail: b.fiedler@tu-harburg.de

T. Hobbiebrunken · M. Hojo
Department of Mechanical Engineering,
Graduate School of Engineering,
Kyoto University, Kyoto, Japan

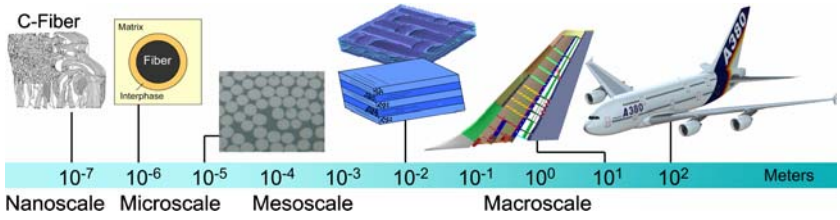


**Fig. 1** Hierarchy in high performance composite materials

where failure takes place. The average stresses and strains may not be sufficient to characterize failure mechanisms of composite materials, although many composite failure theories have been developed based on average macroscopic stresses in a laminate. For example the Tsai-Hill and Tsai-Wu [11] failure criteria are based on the average stresses within a laminate. The mechanisms of initial composite failures are characterized as localized matrix plasticity and micro damage. The study of such details of mechanical behaviour of heterogeneous media is called micromechanics.

One of the most elegant ways to bridge different scales in a calculation of composite stresses and strains is the homogenization method. The homogenization method provides microscopic stresses and strains under macroscopic loads. Once the microscopic field variables are known, matrix and interface failure criteria can be applied to predict composite failure. The homogenization method is used in this work to analyze the stress and strain on the composite microscale at the moment of experimentally observed failure initiation. In a former work we investigated the failure initiation process by in-situ observations in a scanning electron microscope (SEM). The results will be briefly shown in Section 'In-situ failure observation'.

## In-situ failure observation

### Materials and Specimens

The considered composite consists of epoxy resin (RTM6, Hexcel corp.) and carbon fibres (HTA 5131 6 K, Toho Tenax). The RTM6 specimens were manufactured in a vacuum assisted transfer moulding (RTM) process. After resin infusion at 110°C, the resin was cured at 180°C for 2 h under an applied pressure of 0.7 MPa. A detailed explanation of the specimen manufacturing procedure is given in [12].

Three point flexure specimens had a dimension of $3 \times 3 \times 30$ mm$^3$ (width, thickness, length). For the cross ply laminates the general lay-up and the fibre orientation are shown in Fig. 2. Five different lay-ups were chosen [9011], $[904/0_3/90_4]$, $[90_3/0_5/90_3]$, $[90_2/0_7/90_2]$, and $[90_1/0_9/90_1]$.

### Experimental results

In the present paper, we investigated the influence of the different laminate lay-ups on the occurrence of initial matrix cracks. We found that initial failure was difficult to observe in specimens with a high 90°/0°-layer ratio, because ultimate failure occurred without any initial cracks. In particular it was impossible to observe initial failure in the HTA/RTM6 $[90_{11}]$- and $[90_4/0_3/90_4]$-laminates. On the other hand it was easier to observe initial cracks in specimens with a lower 90°/0°-layer ratio. The reason was that the 90°-layer was restrained by the rather stiff 0°-layer.

Figure 3 shows initial failure in a HTA/RTM6 laminate $[90_2/0_7/90_2]$. An arrow indicates the loading direction (direction of macroscopic tensile stress). The images were taken at the 90°-layer region at the tensile side of the bending specimen close to the 0° boundary. A magnification before and after failure initiation is shown on the right side. The image after failure initiation shows two initial cracks at the interface where the fibres have their closest interfibre distance (marked by white ovals). The interface failed preferably between neighbouring fibres in which the centre-to-centre line is parallel to the loading direction. The image before failure initiation shows that the fibres at the failure location did not directly touch each other. The resin matrix layer between those fibres was about 0.5–1 μm. Further loading caused only a small increase in number of cracks till sudden catastrophic failure.

Interesting is, that initial failure occurred in the specimen close to the lower 0°/90° boundary and not at the bottom surface (tensile side) of the specimen, where we expect the highest tensile stresses. Possibly microscopic

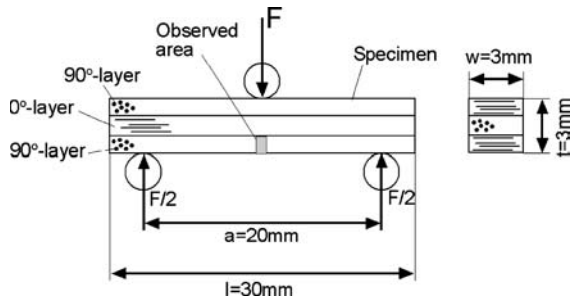


**Fig. 2** Specimen geometry

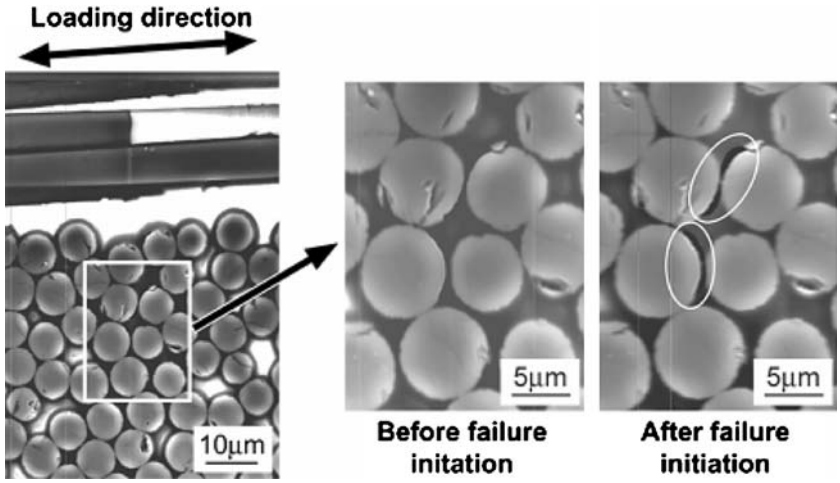


**Fig. 3** Initial crack in HTA/RTM6 composite

effects, like fibre arrangement, are responsible for this phenomenon.

Interfacial failure is the dominating failure mechanism. The fracture surfaces after ultimate failure were investigated using a field emission scanning electron microscope (FE-SEM) for a qualitative evaluation of the interfacial bond. Figure 4a shows of a the surface of a neat carbon fibre and Fig. 4b shows the carbon fibre surface of HTA/RTM6 after ultimate failure. The comparison of Fig. 4a, b shows that in the composite the carbon fibres are almost completely covered with resin. This indicates that the matrix close to the interface has failed. As the folded ribbon structure of the carbon fibres is still visible, the covering resin layer must be very thin (less than 100 nm). The FE-SEM results indicate that the dominating failure mechanism is interphase failure (cohesive) in HTA/RTM6.

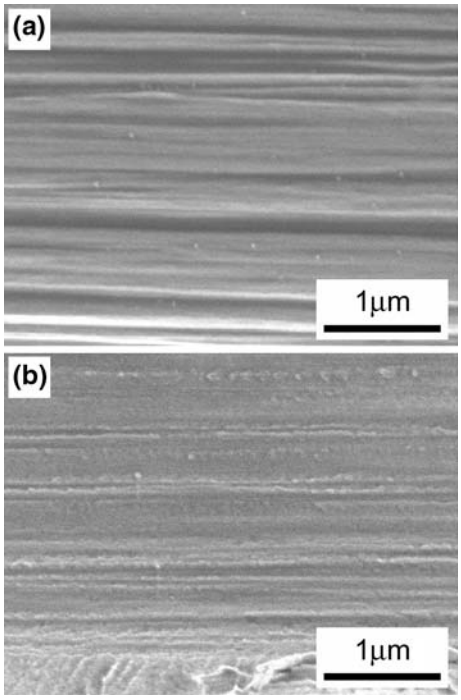


**Fig. 4** Neat C-fibre surface before resin infiltration (**a**) and failed HTA/RTM6 interface (view on C-fibre) (**b**)

## Hierarchical modelling

### Asymptotic expansion

The two-scale homogenization method based on the asymptotic expansion of the field variables was developed for composite materials with periodic internal structures [13]. This approach has been successfully employed not only to solve elastic [14] but also nonlinear [15] multi-scale problems. Moreover, the homogenization method was used for analyzing composites with time-dependent non-linear matrix properties [16] and for the study of fracture in woven fabric composites [17]. An implementation of this method in adaptive finite element analysis was described by Guedes and Kikuchi [18].

In the present analysis we used the commercial finite element software Marc™ (version 2003) with the pre- and postprocessor Mentat™ to carry out the FE-calculations. Figure 5 illustrates the micro/macro-calculation procedure. Assuming a periodic microstructure of the composite ply, the composite can be represented by periodic repeating elements, so called unit-cells. The dimension of the unit-cell is supposed to be much smaller than the macroscopic structure. Define the macroscopic coordinate system with $\mathbf{x} = (x_1, x_2, x_3)$ and the microscopic coordinate system with $\mathbf{y} = (y_1, y_2, y_3)$. They are related by $\mathbf{y} = \mathbf{x}/\varepsilon$, where $\varepsilon$ is the scale ratio. The displacement on the macroscopic scale, $u_i^0(\mathbf{x})$, are calculated by the homogenized model of the bending beam. The displacement on the microscopic scale $u_i$ $(\mathbf{x},\mathbf{y})$ can be written as an asymptotic expansion with respect to $\varepsilon$ [17]:

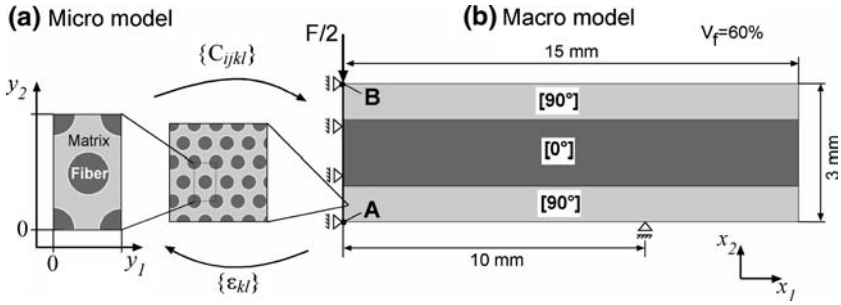


**Fig. 5** Schematic illustration of a two-scale calculation

$$u_i^{\varepsilon}(\mathbf{x},\mathbf{y}) = u_i^0(\mathbf{x}) + \varepsilon u_i^1(\mathbf{x},\mathbf{y}),\ \left(\mathbf{x},\mathbf{y}=\frac{\mathbf{x}}{\varepsilon}\right) \tag{1}$$

In this equation $u_i^1(\mathbf{x},\mathbf{y})$ is Y-periodic and called local perturbation due to the microscopic heterogeneity in the unit-cell.

The displacements of the unit-cell on the microscopic scale can be expressed by (Eq. 2).

$$u_i^{\text{micro}}(\mathbf{y}) = \frac{\partial u_i^0(\mathbf{x})}{\partial x_j} y_j + u_i^1(\mathbf{y}) \tag{2}$$

In this equation $\frac{\partial u_i^0(\mathbf{x})}{\partial x_j}$ is the macroscopic strain and $u_i^1(\mathbf{y})$ is the perturbation on the microscale. Equation 2 was applied to the microscopic unit-cell by constraining the nodes on opposite surfaces of the unit-cell. The macroscopic strains and perturbations where written in a FORTRAN code and implemented into the calculation using a MARC specific subroutine.

## Two-scale modelling

The FE-model of the unit-cell and the bending beam are made by two dimensional 4-node plane strain elements. Owing to symmetry, only one half of the bending beam was modelled. The unit-cell consists of matrix and fibres. We assume a periodic array of the fibres in the matrix. In this case, an area, shown Fig. 5a, is sufficient to represent the microstructure of the composite. The matrix was modelled as an isotropic non-linear plastic material with temperature dependent thermal (coefficient of thermal expansion) and mechanical (Young's modulus and yield stress) properties and the v. Mises criterion was used to predict yielding under tri-axial stress states. The thermo mechanical properties of RTM6 were investigated earlier [19] and the results were applied to the present analysis. The linear elastic matrix and fibre properties are presented in Table 1. The homogeneous composites were assumed to be orthotropic. The homogenized elasticity tensor $C_{ijlk}$ and the thermal properties were calculated from the average stress or displacement in the microscopic unit-cell for an applied strain or temperature change, respectively. The calculated linear elastic composite properties are also given in Table 1.

Since the matrix was considered as a non-linear material, the mechanical response of the unit-cell will also be non-linear for sufficiently large strains. Therefore, the transverse behaviour of the composites has to be considered as non-linear as well. However, a huge amount of computational costs is necessary in order to solve a non-linear micro–macro analysis. Takano et al. [20] proposed a simplified non-linear algorithm, which separates the microscopic and macroscopic analysis. In the first step, the homogenized properties are calculated and stored in a database. The homogeneous calculation is carried out in the following step using the properties stored in the database. We used a similar approach in the present work. The temperature dependency of the Young's modulus, the yield stress, and the non-linear stress strain behaviour were calculated from the unit-cell and incorporated into the homogeneous model.

It is more suitable to describe the stress state in the interface in terms of interfacial normal stress $\sigma_r$ and interfacial shear stress $\tau_{r\theta}$ owing to the fibre. Therefore the acting stresses were expressed in cylindrical coordinates with the centre of the fibre as origin. Then the limiting

**Table 1** Linear elastic mechanical and thermal fibre, matrix and composite properties

| | Fibre (Toho Tenax HTA) | Matrix (RTM6) | Composite ($V_f$ = 60%) |
|---|---|---|---|
| $E_{11}$ [GPa] | 235 | 2.8 | 144 |
| $E_{22}$ [GPa] | 28 | | 9 |
| $E_{33}$ [GPa] | 28 | | 9 |
| $G_{12}$ [GPa] | 24 | 1 | 3.6 |
| $G_{23}$ [GPa] | 7 | | 2.7 |
| $G_{31}$ [GPa] | 24 | | 3.6 |
| $\nu_{12}$ [1] | 0.28 | 0.38 | 0.32 |
| $\nu_{23}$ [1] | 0.33 | | 0.49 |
| $\nu_{31}$ [1] | 0.02 | | 0.03 |
| $\alpha_{11}$ [$10^{-6}$ $K^{-1}$] | –0.1 | 54 | 0.5 |
| $\alpha_{22}$ [$10^{-6}$ $K^{-1}$] | 10 | | 36.2 |
| $\alpha_{33}$ [$10^{-6}$ $K^{-1}$] | 10 | | 36.2 |

strengths are the interfacial normal strength (INS) and the interfacial shear strength (ISS).

## Numerical results

### Macroscopic calculation

In this section the macroscopic stresses in the bending beam are given in Cartesian coordinates where the $x$-direction is the same direction as the fibre direction in the 0°-ply of the cross-ply laminate, Fig. 5. The macroscopic stresses are called $\sigma_1$, $\sigma_2$, and $\sigma_3$, where $\sigma_1$ is that component of macroscopic stress which is of main interest for transverse failure initiation in the 90°-ply.

Macroscopic residual stresses occur in cross-ply laminates as a result of the ply anisotropic coefficient of thermal expansion. The calculated macroscopic ply stresses $\sigma_1$ for all investigated cross-ply laminates are shown in Fig. 6a after cooling and Fig. 6b cooling + loading. The bending stresses were taken at the centre of the beam along the bold line (A–B) in Fig. 5.

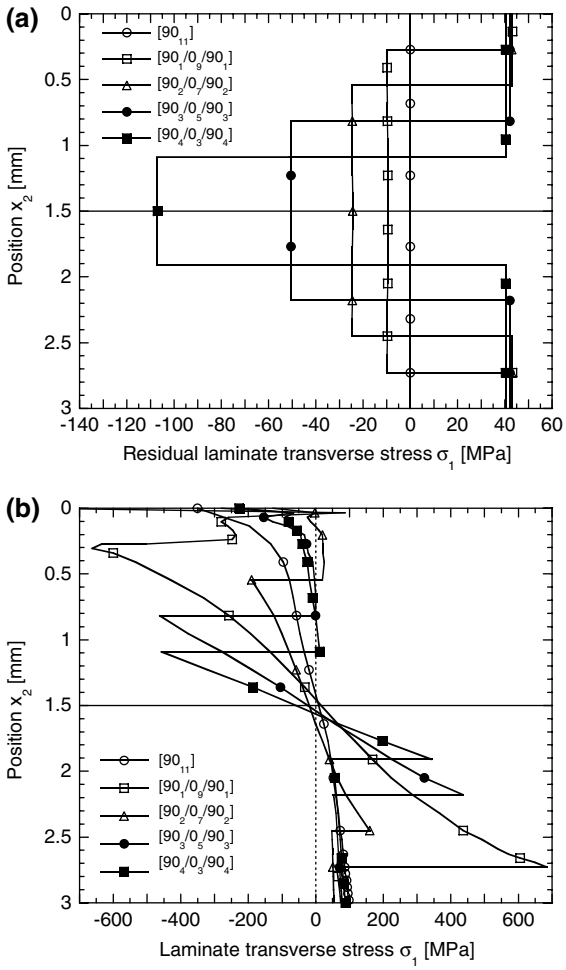


**Fig. 6** Macroscopic residual ply stress distribution in the HTA/RTM6 laminates after cooling (**a**) and after cooling + loading (**b**)

Macroscopic residual stresses do not exist in the $[90_{11}]$-laminate, because a $[90_{11}]$ laminate is macroscopically homogeneous. On the other hand, tensile stresses exist in the 90°-plies and compressive stresses in the 0°-plies for the cross-ply laminates. The macroscopic residual stress distribution changes significantly for different laminate lay-ups, Fig. 6a. However, the maximum residual stresses in the 90°-plies vary only in a small range. The average stress of the cross-ply laminate should be zero, as a result of a macroscopic force balance. This can be seen from the Fig. 6a. The sum of the area under the curve, left and right from the zero stress line, is zero for all laminates. The macroscopic bending stresses below the load line (A–B) are summarized in Fig. 6b. Even though the 90°-plies are the outer plies of the cross-ply laminate, the highest macroscopic stresses occur in the 0°-plies because of their high Young's modulus.

The maximum macroscopic tensile stresses $\sigma_1$ in the 90°-ply of the bending beams after cooling and loading at the moment of initial failure are summarized in the Fig. 7 for all investigated lay-ups. The ultimate failure stress of the 90°-plies are also shown for comparison.

In the case of the HTA/RTM6 $[90_4/0_3/90_4]$-laminate ultimate 90°-ply failure occurred suddenly without any initial cracks. For the other cross-ply laminates, we observed initial failure in the 90°-ply over a wide range of the maximum 90°-ply stress values. In these cases initial failure occurred at a macroscopic stress of 54–78 MPa, which is 54–80% of the maximum 90°-ply failure stress. Residual stresses caused no failure in all specimens. However, initial failure occurs early during mechanical loading in laminates with relatively thin 90°-plies ($[90_1/0_9/90_1]$ and $[90_2/0_7/90_2]$).

The macroscopic strain state at the moment of failure initiation was applied in the microscopic analysis. We assumed that initial failure directly lead to final failure for

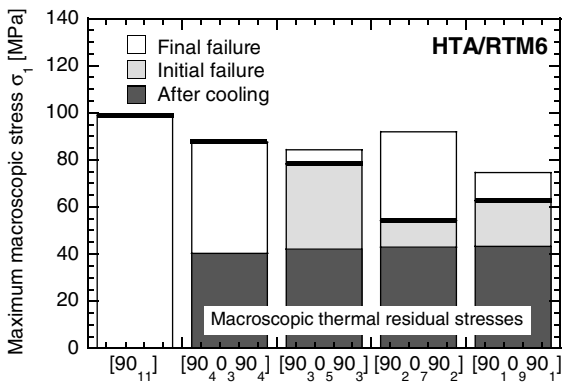


**Fig. 7** Maximum macroscopic residual stresses in the 90°-ply of the HTA/RTM6 laminates after cooling, at initial and at final failure

specimens in which we observed no initial failure. In this case the macroscopic strain state at ultimate 90°-ply failure was used in the micromechanical calculation. The tensile stress in the 90°-plies at initiation of failure is marked with bold lines in Fig. 7.

## Microscopic calculation

The aim of this paper is to calculate the microscopic stress state that causes transverse failure initiation. A micro/macro numerical calculation of the in-situ experiments will provide the stress and strain state at the moment of failure initiation. The maximum interfacial normal $\sigma_r$ and shear $\tau_{r\theta}$ stresses at failure initiation will be calculated and analyzed.

Figure 8 shows the stress pattern of $\sigma_r$ and $\tau_{r\theta}$ in the matrix of the HTA/RTM6 $[90_{11}]$ and $[90_2/0_7/90_2]$ laminates after cooling and at the moment of failure initiation (cooling + loading). It can be seen that the presence of the 0°-plies cause a similar microscopic radial and shear stress distribution after cooling is similar to an applied transverse load. The maximum $\sigma_r$ after loading occur in 0°-direction, which is the direction of the macroscopic tensile stress $\sigma_1$. This is also the direction of the maximum radial stress after cooling in the cross-ply laminates. Thermal residual stresses and the difference in elastic properties cause a stress concentration at this location [21]. The absolute maximum shear stresses develop in the 33°-direction.

The resulting maximum interfacial normal and shear stresses in all investigated laminates are summarized in Table 2 (after cooling) and Table 3 (after cooling + loading). The microscopic residual radial stresses vary from –3 MPa $[90_{11}]$ to 43 MPa $[90_4/0_3/90_4]$ and the maximum interfacial shear stresses are between 4 MPa $[90_{11}]$ and 25 MPa $[90_1/0_9/90_1]$.

The microscopic interfacial stress values at the moment of initial failure vary from 86 to 150 MPa. Thus, the maximum radial stresses are about 1.52–1.7 times of the macroscopic ply stress. The maximum shear stresses are between 34 and 48 MPa.

A comparison of the interfacial stresses shown in Fig. 9, with the SEM observations of initial failure, Fig. 3, gives the following conclusion. As we mentioned initial failure occurs always at the location of highest stress concentration. Fig. 3 shows initial cracks in HTA/RTM6. The location of initial failure is equivalent with the location at the interface for $\alpha = 0°$ in our finite element model. The interfacial normal stresses are maximum and the interfacial shear stresses are almost zero at this location, as shown in Fig. 9 for the microscopic calculation of the HTA/RTM6 $[90_2/0_7/90_2]$ laminate. Thus, we conclude that the interfacial shear stresses are insignificant for failure initiation. This conclusion can also be derived independently from the location of interfacial failure by comparing the maximum interfacial shear stresses with interfacial shear strength obtained by the microdroplet shear test [22]. The maximum

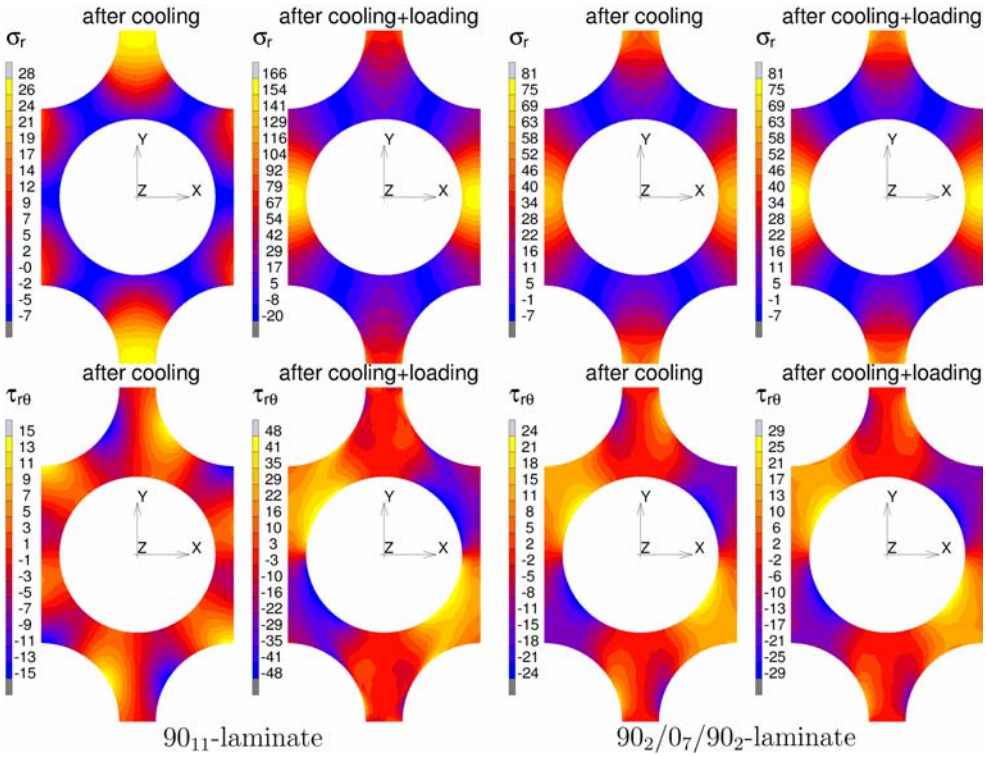


**Fig. 8** Radial stress pattern in the $[90_{11}]$ and $[90_2/0_7/90_2]$-laminate after cooling and after bending

**Table 2** Maximum macroscopic and microscopic stresses after cooling ($\Delta T$ = –155°C)

| Lay-up | Max macroscopic residual stress [MPa] | Max interfacial normal stress [MPa] | SCF [MPa] | Max interfacial shear stress [MPa] |
|---|---|---|---|---|
| $[90_{11}]$ | – | –3 | – | 4 |
| $[90_4/0_3/90_4]$ | 40 | 51 | 1.28 | 22 |
| $[90_3/0_5/90_3]$ | 42 | 56 | 1.34 | 24 |
| $[90_2/0_7/90_2]$ | 43 | 58 | 1.35 | 24 |
| $[90_1/0_9/90_1]$ | 43 | 61 | 1.42 | 25 |

**Table 3** Maximum macroscopic and microscopic stresses after cooling and loading at the moment of initial failure

| Lay-up | Max macroscopic tensile stress [MPa] | Max normal stress [MPa] | SCF [MPa] | Max interfacial shear stress [MPa] |
|---|---|---|---|---|
| $[90_{11}]$ | 99 | 150 | 1.52 | 48 |
| $[90_4/0_3/90_4]$ | 85 | 143 | 1.68 | 48 |
| $[90_3/0_5/90_3]$ | 78 | 133 | 1.7 | 46 |
| $[90_2/0_7/90_2]$ | 54 | 86 | 1.6 | 34 |
| $[90_1/0_9/90_1]$ | 75 | 105 | 1.4 | 41 |

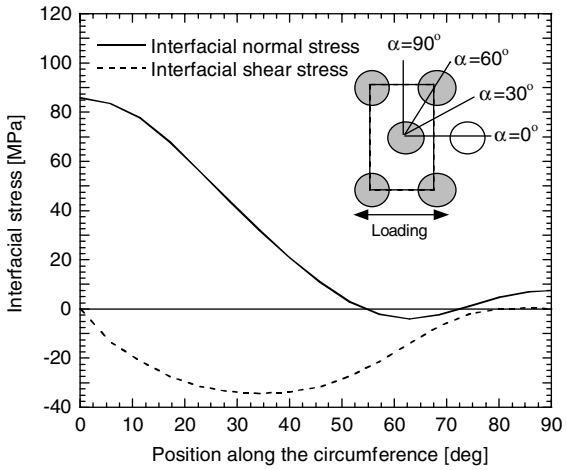


**Fig. 9** Interfacial stress pattern in the hexagonal unit-cell at the location of initial failure in the $[90_2/0_7/90_2]$-laminate

interfacial shear stresses at the moment of interfacial failure are much lower (34–48 MPa) than the interfacial shear strength ($\tau_{r\theta f}$ = 156 MPa). This led us to the conclusion that the interfacial normal stress governs the failure initiation under transverse loading, with the assumption of a hexagonal fibre array. However, the SEM-observations showed, that the fibre-arrangement is more irregular. This can affect the microscopic stress distribution. The influence of the fibre distribution will be studied in a future work [23].

## Conclusion

Interfacial failure in a high performance carbon fibre epoxy resin composite was investigated by in-situ experiments and numerical calculations. In-situ observations provide important information about transverse failure initiation and crack propagation. The use of cross-ply laminates turned out to be useful, since the tensile stress in the 90°-ply is controlled but the rather stiff 0°-ply. The onset of failure and the failure process could successfully observed in the SEM. These observations showed that failure always initiates at the fibre/matrix interface in the closest distance to the neighbouring fibre and direction of macroscopic tensile load. A non-linear finite element analysis provided quantitative values of the interfacial stresses at the location of initial failure. Comparisons of our experimental and numerical results lead to the conclusion that the interfacial normal strength governs the initiation of failure in composites under transverse load.

**Acknowledgements** This work was supported in the frame of the collaborative program of the German Research Foundation (DFG) and the Japan Society for Promotion of Science (JSPS).

## References

1. Lakes R (1993) Nature 361:511
2. Baer E, Hiltner A, Keith HD (1987) Science 235:1015
3. Voigt W (1910) Teubner
4. Reuss A (1929) Ztschr f Angew Math Mech 8:161
5. Hill R (1965) J Mech Phys Solids 13:189
6. Paul B (1960) Trans Metal Soc AIME 218:36
7. Hashin Z, Rosen BW (1964) J Appl Mech 32:223
8. Hill R (1964) J Mech Phys Solids 12:199
9. Aboudi J (1989) Appl Mech Rev 42:193
10. Adams DF, Doner DR (1967) J Composite Mater 1:153
11. Tsai SW, Wu EM (1971) J Composite Mater 5:58
12. Hobbiebrunken T, Hojo M, Adaji T, de Jong C, Fiedler B (2004) Composite Part A (in press, Available online 28 February 2006)
13. Sanchez-Palencia E (1980) Non-homogeneous media and vibration theory. Springer, Berlin, p 45
14. Fish J, Shek K (2000) Compos Sci Technol 60:2547
15. Jansson S (1992) Int J Sol Struc 29:2181

16. Wu X, Ohno N (1999) Int J Sol Struc 36:4991
17. Takano N, Uetsuji Y, Kashiwagi Y, Zako M (1999) Mater Sci Eng 7:207
18. Guedes JM, Kikuchi N (1990) Comput Methods Appl Mech Eng 83:143
19. Hobbiebrunken T, Hojo M, Fiedler B, Tanaka M, Ochiai S, Schulte K (2004) JSME Int J Ser A 47:349
20. Takano N, Ohnishi Y, Zako M, Nishiyabu K (2001) J Sol Struc 38:6333
21. Fiedler B, Hojo M, Ochiai S, Schulte K, Ochi M (2001) Compos Sci Technol 61:95
22. Hobbiebrunken T (2005) Microscopic transverse failure initiation in composite materials – an interdisciplinary multi-scale research. Doctor Thesis, Kyoto University
23. Hobbiebrunken T, Hojo M, Jin KK, Oh JH, Ha S (submitted) J Composite Mater